ELSEVIER

International Journal of Mass Spectrometry 219 (2002) 343–350

International Journal of Mass Spectrometry

www.elsevier.com/locate/ijms

XY-TOF technique for large ion source mass spectrometers

T. Jalowy[a], R. Neugebauer[a], K.O. Groeneveld[a], C.R. Ponciano[b], L.S. Farenzena[b], E.F. da Silveira[b,*]

[a] *Institut für Kernphysik der J.W. Goethe Universität, August-Euler-Str. 6, D-60486 Frankfurt am Main, Germany*
[b] *Departamento de Física, Pontifícia Universidade Católica, CP 38071, Rio de Janeiro 22452-970, Brazil*

Received 14 February 2002; accepted 30 May 2002

Abstract

The combination of time-of-flight (TOF) with two-dimensional position-sensitive (*XY*) ion detection techniques is employed to increase detection sensitivity of gas mass spectrometers. For this, the length of ion sources is significantly increased without deteriorating the mass resolution; this is achieved by using the *XY* information to correct the TOFs of the ions produced in the collisions. The ion dynamics expressions for such *XY*-TOF method are deduced. The gas pressure may be kept at a uniform value all over the cell to facilitate accurate absolute measurements. Experimental results of 150 keV neutral H (H^0)-beam colliding with a He–Ne–Ar mixture are shown before and after the *XY*-TOF compensation. (Int J Mass Spectrom 219 (2002) 343–350)

Keywords: TOF; *XY*-TOF; Gas target; Position-sensitive detection; Mass spectrometry

1. Introduction

Gas spectrometry based on time-of-flight (TOF) analysis has been developed long time ago [1–5]. Wiley and McLaren [3] introduced in 1955 the time-focusing principle in a two-acceleration-region linear spectrometer. Essentially, they designed the instrument in such a way that the ion time of flight does not depend, in first order approximation, on the finite size of the ionized region. To further improve mass resolution, sensitivity or dynamical range of gas spectrometers, new techniques have been added: pulsed extraction fields [6], ion lenses, electrostatic mirrors [7] or guides [8], position-sensitive detectors [9–11], etc.

Beam-profile monitoring associated with residual gas analysis has been already achieved by employing the combination of TOF and two-dimensional position-sensitive (*XY*-TOF) detection techniques [12]. In this method, two sets of *XY* detectors are placed in each side of the beam, respectively. After ionization of the residual gas by the projectiles, the recoiling positive ions and the emitted electrons are accelerated towards the detectors by an electric field perpendicular to the beam direction. The beam profile in the plane parallel to the detectors is given directly by the *XY* impact coordinates of the ions, while the profile in *Z* direction is given by TOF differences between ion detection and electron detection.

In this article, such *XY*-TOF combination is analyzed for a different geometry (the beam is oblique to the detectors) and the goal is to keep constant the spectrometer resolution power while its gas cell volume is increased. Now, the *XY* information is not employed to inform about the beam profile, but to compensate

* Corresponding author. E-mail: enio@fis.puc-rio.br

1387-3806/02/$ – see front matter
PII S1387-3806(02)00735-2

the TOF values of the ions having the same mass and produced at different distances of their detector. This compensation may be interpreted as an algorithm to transform exactly (and not only in first order approximation) the obtained experimental data into new ones, corresponding to a virtual set-up in which the ionizing beam is perpendicular to the spectrometer axis. The combination of *XY*-TOF ion detection techniques is employed to increase overall detection sensitivity of gas mass spectrometers. Moreover, the method facilitates accurate absolute measurements because the gas pressure may be kept at a uniform value all over the cell. This represents an advantage over instruments using highly space focusing optics into gas jet targets.

After describing the basic equations and the experimental set-up, the method is applied for analyzing a gas mixture in a 4.1-cm long ionization region.

2. Theoretical background

2.1. TOF equations

As shown in Fig. 1, the *XZ* plane is defined by the beam trajectory (incidence angle θ_p) and by the spectrometer symmetry axis. The ionization occurs at the projectile (p) coordinates x_p, $y_p = 0$, $z_p = x_p$ cotg θ_p and at time $t_p = x_p/(v_p \sin\theta_p)$ before the projectile crossing the electrode 1, where v_p is the projectile velocity. The ion detection time, T, is defined as the time interval between the $x = y = z = 0$ crossing and the detection of the gas ion events; therefore, $T + t_p$ is the TOF for a given ion.

Two uniform acceleration regions are defined by the electrode 1 (a metal plate biased at potential U_1), the electrode 2 (a high transmission grid at potential U_2), and the *XY* ion detector with a grounded entrance surface. The gas molecule ion is emitted with velocity v_0 in the direction given by the angle θ with the *Z*-axis, in a plane forming an angle φ with the *XZ* plane, and reaches the grounded detector surface at the detector (D) coordinates:

$$x_D = x_p + v_0(T + t_p)\sin\theta\cos\varphi$$
$$y_D = v_0(T + t_p)\sin\theta\sin\varphi$$
$$z_D = d_1 + d_2. \quad (1)$$

Considering respectively t_1 and t_2 as the TOFs in the first and second acceleration regions, the ion detection time T, with respect to the moment the projectile

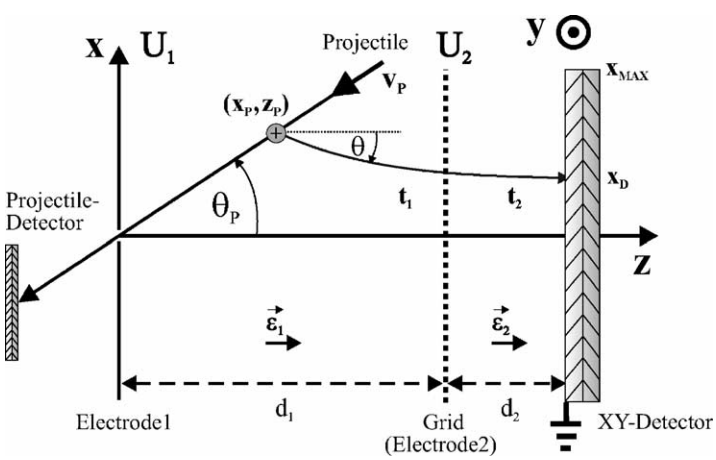

Fig. 1. Two-acceleration-field cylindrical spectrometer. The projectile arrives in the *XZ* plane and crosses the origin $x = y = z = 0$ at the time $T = 0$. The gas ion is produced at the point (x_p, $y_p = 0$, z_p) at the time $-t_p$ and is emitted with velocity v_0 in a direction given by the angle θ with respect to *Z*-axis. A grid separates the first acceleration region from the second one. The x_{max} is the detector radius and x_D is the coordinate of the ion impact point on the detector surface. The electric field components ε_x and ε_y are kept at zero; ε_z is constant inside each sub-region.

arrives at the end of the gas cell, is:

$$T = t_1 + t_2 - t_p = \frac{d_1 - z_p}{(v_{0z} + v_{1z})/2} + \frac{d_2}{(v_{1z} + v_{2z})/2} - \frac{z_p}{v_p \cos\theta_p} \quad (2)$$

$$T' = \sqrt{m}\left[\frac{2d_1}{\sqrt{3kT_G}\cos\theta + \sqrt{3kT_G\cos^2\theta + 2q(U_1 - U_2)}} + \frac{2d_2}{\sqrt{3kT_G\cos^2\theta + 2q(U_1 - U_2)} + \sqrt{3kT_G\cos^2\theta + 2qU_1}}\right] \quad (6)$$

where v_{0z}, v_{1z}, and v_{2z} are the axial velocities of the ionized gas molecule at the collision, grid crossing, and detector arrival times, respectively. These velocities are given by:

$$v_{0z} = v_0 \cos\theta \quad (3)$$

$$v_{1z} = \sqrt{v_{0z}^2 + \frac{2q}{m}(U_1 - U_2)\left(1 - \frac{z_p}{d_1}\right)} \quad (4)$$

$$v_{2z} = \sqrt{v_{1z}^2 + \frac{2q}{m}U_2} \quad (5)$$

These expressions hold for tg $\theta_p > x_{max}/d_1$, a condition which guarantees that ionization should occur only in the first acceleration region. If no post-acceleration or no drift-region is needed, d_2 and U_2 may be set to zero and electrode 2 becomes the ion detector itself.

Considering the momentum transfer from the projectile to gas molecule to be negligible [13], the thermal velocity component dominates and the produced ion of mass m has an average velocity given by $(v_0)_{rms} = \sqrt{3kT_G/m}$; where T_G is the gas temperature.

2.2. Transformation for narrowing TOF peaks of the gas ions

The TOF peaks are broad mainly because ions are produced along the track at different distances from the detector. A numerical transformation with the event-by-event *XY*-TOF data (i.e., the experimental data set: x_D^{exp}, y_D^{exp}, and T_D^{exp}) can eliminate this dependence by simulating that: (i) the target gas inside the ion source is totally compressed over the electrode 1, and (ii) the ionizing beam enters in the ion source perpendicularly to the spectrometer axis and through the gas compressed layer. The new TOF T' has its zero at the instant of the beam–gas molecule collision.

Under these conditions, T' writes:

The orthogonal beam configuration reduces strongly the T' peak broadening: the residual TOF dispersion is due to convolution over the beam thickness and over the different emission angle θ. A good approximation for describing the average value of T' is obtained substituting $\sqrt{3kT_G}\cos\theta$ by its average value (zero) and neglecting $3kT_G\cos^2\theta$ with respect to the electrostatic energies. Eqs. (2) and (6) are then employed to create a numerical algorithm for narrowing the gas peaks, in which T', the theoretical TOF of ions formed at $x_p = 0$, is divided by $T(x_D^{exp})$, the theoretical TOF (corrected by the time t_p) of ions formed at $x_p = x_D^{exp}$. So, the transformation $T(x_D) \rightarrow T'$ consists in multiplying, for each ion detected at the position x_D^{exp}, the experimental value T_D^{exp} by the function $F(x_0^{exp})$ defined by:

$$F(x_D^{exp}) = \frac{T'}{T(x_D^{exp}) + x_D^{exp}/v_p \sin\theta_p} \quad (7)$$

Fig. 2 illustrates the $x_D(T)$ and $x_D(T')$ plots calculated for a mixture of three noble gases (He, Ne, and Ar) ionized by a 150 keV neutral H (H^0)-beam. The projection of each of these plots over the TOF abscissa generates the usual TOF spectrum.

Finally, two points should be emphasized:

(a) Eq. (6) shows that it is possible to define a *reduced TOF* as $T'_{red} = T'/\sqrt{m}$. Therefore, the different $x_D(T'_{red})$ curves for each gas molecule mass are reduced towards a universal one in which the non-homogeneities of the acceleration field acting over all ion species show up in the same manner [14]. Eventual discrepancies with respect to this universal curve should reveal specificities of the

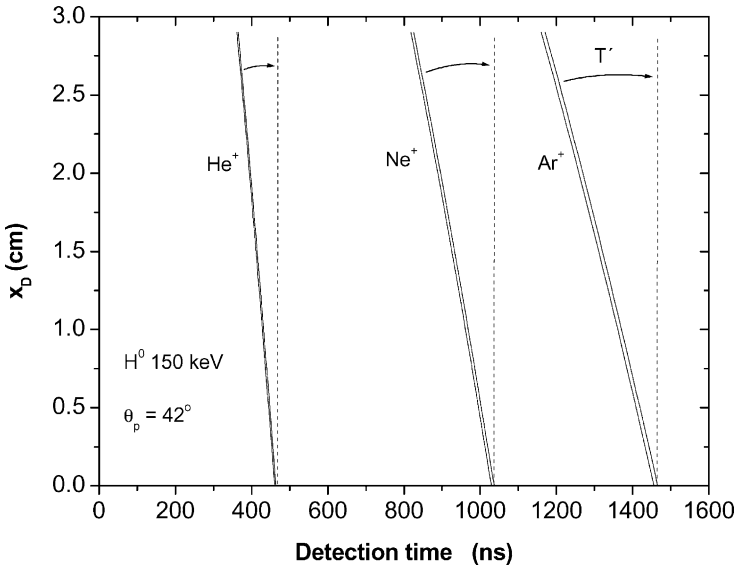

Fig. 2. The plots $x_D(T)$ and $x_D(T')$ calculated for a mixture of three noble gases (He, Ne, and Ar) under ionization by a 150 keV H^0-beam. The detection time is the gas ion TOF ($t_1 + t_2$) subtracted the time necessary for the projectile to reach the electrode after the gas molecule collision (t_p). The calculation for $\theta = 0^\circ$ and $\theta = 180^\circ$ simulates the line broadening due to thermal movement of the gas.

collision between the beam and a particular gas species.

(b) The mass resolution may be further improved by cooling down the gas (reducing the average velocity of gas molecules) and/or using a strongly collimated beam. An elegant solution for systems using thick beams would be to install another *XY* anode for the start detector for determining the parameters of each projectile trajectory and including them in the $T(x_D) \rightarrow T'$ transformation.

3. Experimental

A gas *XY*-TOF spectrometer, described elsewhere [11], was filled with 70% He, 15% Ne (i.e., 13.6% ^{20}Ne and 1.3% ^{22}Ne), and 15% Ar gas at 10^{-5} mbar total pressure. The monoatomic gases were chosen to avoid Coulomb explosion after their ionization. The mixture was bombarded with a 150 keV H^0-beam produced by the Van de Graaff accelerator of the Institute für Kernphysik of the J.W. Goethe University. Start signals for the TOF system were given by a secondary electron detector placed behind a thin foil covering the central hole of electrode 1. However, because secondary ions are emitted towards the *XY*-detector, best alternatives are to detect behind the small hole: (i) directly the beam (see Fig. 1) or (ii) secondary electrons emitted by a thin foil off-center; care must be taken to avoid sensible field distortion near the hole [14].

The spectrometer parameters for these measurements were: $U_1 = 2.970$ kV; $U_2 = 0.040$ kV; $d_1 = 8.35$ cm; $d_2 = 0.70$ cm, and $\theta_p = 42^\circ$. The beam diameter was about 10^{-2} cm. Gas temperature T_G was about 300 K, so that $(v_0)_{rms} \approx 2.7/\sqrt{m}$ μm/ns, where m is the molecular mass in u units.

Fig. 3a and b represent respectively the measured $x_D(T)$ plot and its projection, the usual TOF spectrum. One sees clearly the curves corresponding to the $^4He^+$, $^{20}Ne^+$ $^{22}Ne^+$, $^{40}Ar^+$, as well as some of their higher charge states. The line thickness is

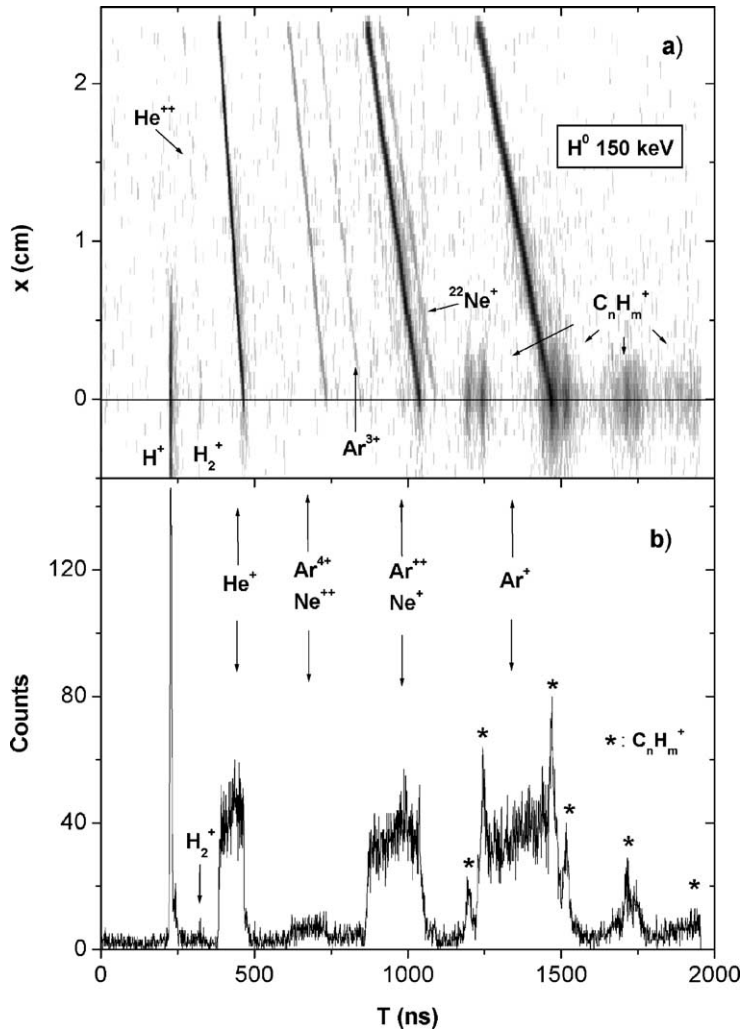

Fig. 3. (a) Experimental $x(T)$ spectrum of He, Ne, and Ar gases bombarded by 150 keV H^0-beam. Incidence angle is $\theta_p = 42^\circ$. Events from the beam–gas collision generate oblique lines for $x > 0$. The points close to the T-axis ($x = 0$ line) and forming vertical lines are due to secondary ions emitted by electrode 1. (b) TOF spectrum, i.e., projection of the $x(T)$ data on the T-axis. The thin peaks are due to the ions desorbed from the electrode, while the gas ions generate the broad peaks.

attributed to the thermal motion of the gas molecules, each point corresponding to the detection of an ion produced by the beam–gas collision. Oblique lines are formed by ions from the gas, while vertical lines are generated by ions emitted from the electrode 1 with relatively large radial velocity. As shown in Fig. 3b, the projection over T-axis of data corresponding to ions produced in the gas or emitted by the electrode surface give rise, respectively, to broad and narrow peaks.

Fig. 4 exhibits the same data shown in Fig. 3 but modified by the $T(x_D) \rightarrow T'$ transformation. The oblique and vertical lines in Fig. 3a became the vertical and oblique ones in Fig. 4a, respectively. The

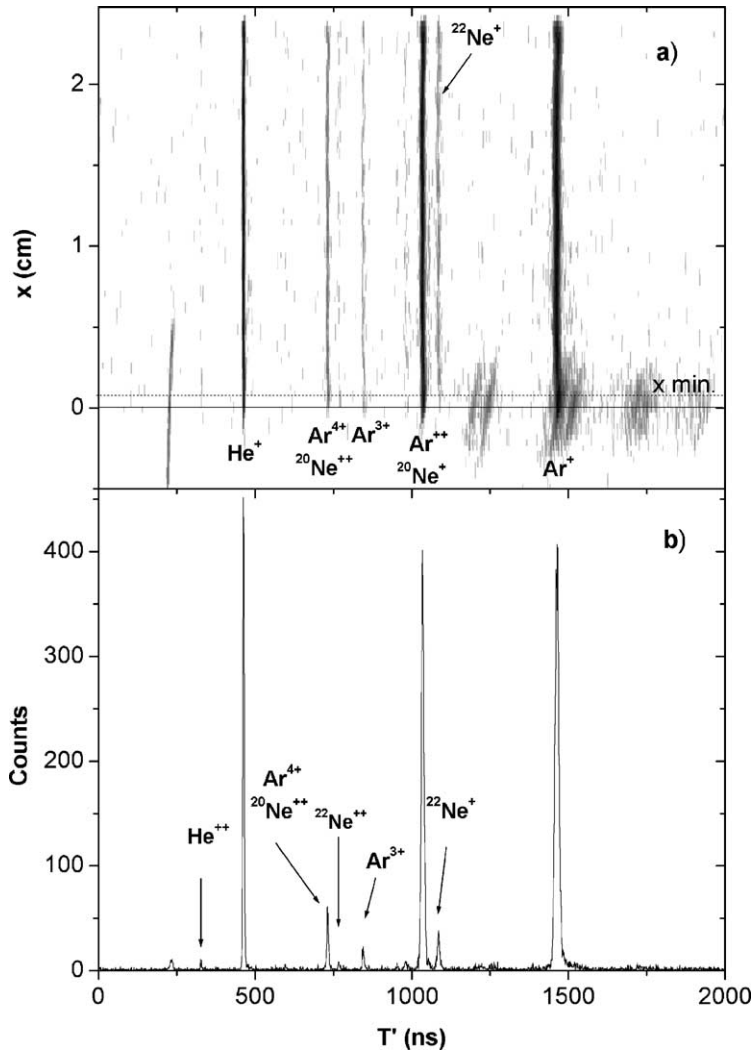

Fig. 4. The same as Fig. 3, but T_D^{exp} for each event has been replaced by $T' = F(x_D^{exp})\, T_D^{exp}$. Note that, for collision in gas, the $T(x_D) \rightarrow T'$ transformation makes possible to display the distribution of points in vertical lines, whose projection results now in narrow TOF peaks.

projection, in Fig. 4b, shows a broader and smaller H^+ peak, while the gas peaks are quite narrow and higher. Small peaks, such as those relative to $^{22}Ne^+$ and $^{20}Ne^{2+}$, or very small ones like He^{2+} and $^{22}Ne^{2+}$, are now visible. Sensitivity can be enhanced further in *XY*-TOF spectra by imposing restrictions on coordinates x_D^{exp} and y_D^{exp} : as all events of interest must occur very close to the *YZ* plane and for positive x_D^{exp}, the others can be eliminated in the transformation for lowering the background. Because the partial pressure of each gas species is constant, the use of geometrical restrictions do not alter the relative yield of the gas ions. Fig. 5 illustrates a $y_D(T)$ plot, from which are extracted the upper and lower values of y_D^{exp} to be used in the selection of the events close to the *T*-axis. In the spectrum shown in Fig. 4b, the limiting values for both coordinates are $-0.05 < y_D^{exp} < 0.15$ and $0.05 < x_D^{exp} < 2.5$ cm, respectively.

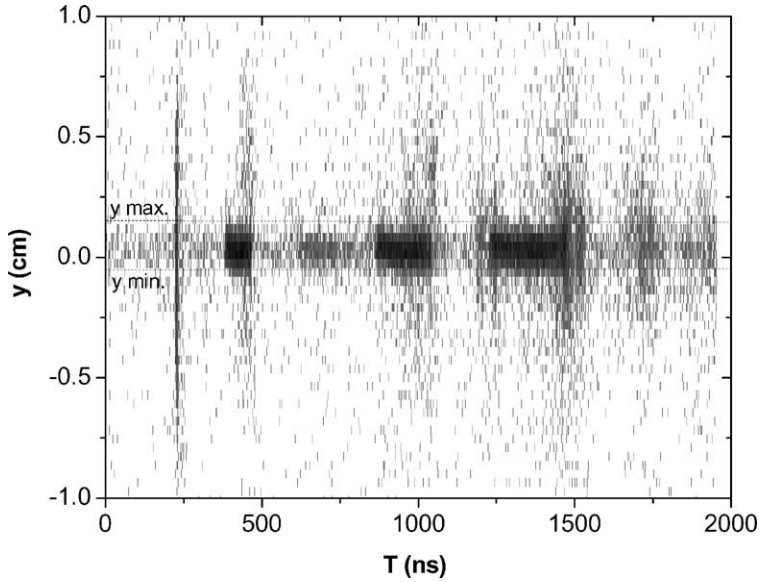

Fig. 5. The $y_D(T)$ plot. It represents, for all events, the y-coordinates of the ion impact on the detector as a function of the ion TOF. Ionized gas molecules have small radial velocities and must reach the detector close to $y = 0$; on the other hand, secondary ions from the electrode often have larger radial velocity. The dashed lines show the y-coordinate limits (y_{min} and y_{max}) used by the software to reduce the contribution from the solid and enhance the gas TOF peaks in Fig. 4.

4. Conclusion

A method is proposed and demonstrated to avoid peak spread-out by compensating the TOF of ions produced along the beam track in gases inside large ion sources. Experimental results show a dramatic improvement of the mass resolution power of the spectrometer when the *XY*-TOF correction is applied. The high sensitivity of the method is demonstrated by identifying He^{2+} and $^{22}Ne^{2+}$ peaks from a mixture of three noble gases.

Acknowledgements

The DAAD/CAPES–PROBRAL program is gratefully acknowledged for making possible the collaboration between IKF and PUC-Rio. PADCT and FAPERJ are also acknowledged for their partial support of the investigations.

References

[1] R.J. Cotter (Ed.), Time-of-Flight Mass Spectrometry, ACS Professional Reference Books, Washington, D.C., 1997.
[2] B.A. Mamyrin, Int. J. Mass Spectrom. Ion Processes 206 (2001) 251.
[3] W.C. Wiley, I.H. McLaren, Rev. Sci. Instrum. 26 (1955) 1150.
[4] J.H. Beynon (Ed.), Mass Spectrometry and its Applications to Organic Chemistry, Elsevier Publishing Company, Amsterdam, 1960.
[5] E.W. Schlag (Ed.), Int. J. Mass Spectrom. Ion Processes 131 (1994).
[6] M.L. Vestal, P. Juhasz, S.A. Martin, Rapid. Commun. Mass Spectrom. 9 (1995) 1044.
[7] V.I. Karataev, B.A. Mamyrin, D.V. Shmikk, JETP 37 (1973).
[8] K.V. Davis, E.F. da Silveira, E.A. Schweikert, Nucl. Instrum. Methods A273 (1988) 203.
[9] O. Becker, K. Wien, Nucl. Instrum. Methods B16 (1986) 456.
[10] M. Most, K. Wien, A. Brunelle, S. Della Negra, J. Depauw, D. Jacquet, M. Pautrat, Y. LeBeyec, Nucl. Instrum. Methods Phys. Res. B168 (2000) 203.
[11] T. Jalowy , R. Neugebauer, M. Hattass, J. Fiol, F. Afaneh, J.A.M. Pereira, E.F. da Silveira, H. Schmidt-Böcking, K.O.

Groeneveld, Nucl. Instrum. Methods Phys. Res. B 193 (2002) 792.
[12] M. Unverzagt, H.E. Berg, J Ulrich, B. Franzke, W. Bourgeois, R Mann, H. Schmidt-Böcking, GSI Annual Report (1992) 449.
[13] M.A. Abdallah, C.R. Vane, C.C. Havener, D.R. Schultz, H.F. Krause, N. Jones, S. Datz, Phys. Rev. Lett. 85 (2000) 278.
[14] T. Jalowy, R. Neugebauer, K.O. Groeneveld, C.R. Ponciano, L.S. Farenzena, E.F. da Silveira, Rev. Sci. Instrum (2002), in press.